UNIVERSIDADE DE SÃO PAULO

INSTITUTO DE FÍSICA
CAIXA POSTAL 20516
01498 - SÃO PAULO - SP
BRASIL

PUBLICAÇÕES

IFUSP/P-937

ONSET OF CHAOTIC FIELD LINE TRAJECTORIES IN TOKAMAKS

Maria Vittoria A.P. Heller and **Iberê L. Caldas**
Instituto de Física, Universidade de São Paulo

Setembro/1991

ONSET OF CHAOTIC FIELD LINE TRAJECTORIES IN TOKAMAKS*

Maria Vittoria A.P. Heller and Iberê L. Caldas

Instituto de Física, Universidade de São Paulo
C.P. 20516, 01498 – São Paulo, S.P., Brazil

Abstract

The onset of chaotic field line trajectories on tokamak plasmas perturbed by external resonant helical currents has been investigated. The spatial distribution of field lines is obtained integrating numerically the differential equations for the perturbed field lines and investigating the Poincaré map characteristics of these fields. Several algorithms have been computed to indentify the transition to chaos for this quasi–integrable dynamical system, which, for a given mhd equilibrium, is determined by the enhancement of the coupling between the helical perturbation and the toroidicity, as the helical current increases.

* Work partially supported by CNPq and FINEP.

1. Introduction

It is well known that a set of closed, nested, toroidal magnetic surfaces is a necessary condition for confining plasmas in tokamaks[1,2]. However, in most experiences, these surfaces can be partially destroyed by resonant helical fields due to plasma oscillations[3] or external perturbations, created by resonant helical windings (rhw) [4] or magnetic limiters[5]. The superposition of these helical perturbations upon an equilibrium with axial symmetry brakes the symmetry of the magnetic field which becomes nonintegrable[1,6,7]. In tokamaks, the amplitudes of these perturbations are so small, as considered in this article, that the perturbed field can be considered an almost integrable system[8]. As a consequence of this fact, perturbational theories can be used to analyse the onset of magnetic islands and stochastic regions, and to investigate the properties of field line trajectories[7].

Since the early experiments with rhw on the Pulsator[4], these external coils have been used in some tokamaks[3,10] to generates helical perturbations in order to control plasma oscillations and to investigate the nature of disruptive intabilities, which deteriorate the plasma confinement in these devices. For a given magnetohydrodynamic (mhd) equilibrium, the helical current intensity determines the magnetic islands widths and the extend of the chaotic regions, which may trigger plasma disruptions[11], as it was suggested in reference (12).

In this article, we deal with alterations on the topology of the tokamak field lines, specially the onset of chaotic field line trajectories, caused by resonants perturbations created by external currents flowing on helical windings wound on a tokamak vessel. The distribution of field lines is obtained integrating numerically the differential equations for the perturbed field lines and investigating the characteristics of the Poincaré maps of these fields. The investigation was done for a large aspect–ratio tokamak in which perturbed magnetic field can be described as an almost integrable system. Here, we report the

modifications caused on the Poincaré maps of that dynamical system as the external helical current – a relevant control parameter in the mentioned experiences – changes.

The mhd equilibrium and the helical perturbations are introduced in section 2. In section 3 the superposition of the helical windings on the equilibrium is considered, being analyzed the magnetic surfaces destruction and the onset of chaotic field lines. The conclusions are given in section 4.

2. Almost Integrable Magnetic Fields in Tokamaks

In this section we introduce the magnetic field $\vec{B}$ produced by the superposition of the tokamak mhd equilibrium field $\vec{B}_0$ with the perturbation field $\vec{B}_1$ created by m pairs of resonant helical windings wound on the tokamak vessel (fig. 1):

$$\vec{B} = \vec{B}_0 + \vec{B}_1 \quad . \tag{1}$$

This superposition is justified by the fact that the helical current intensity I is much lower than the plasma current intensity I_p ($I/I_p \approx 1 \times 10^{-2}$), and therefore $\vec{B}_1$ can be treated in eq. (1) as a small perturbation whose main effect is the creation of magnetic islands around the resonant non perturbed magnetic surfaces.

We consider a toroidal camera with circular cross–section and assume the tokamak scaling

$$\frac{B_{0\theta}}{B_{0_z}} \approx \frac{n\,a}{mR} \ll 1 \quad , \tag{2}$$

valid for large aspect–ratio tokamaks, i.e.,

$$\epsilon = \frac{a}{R} \ll 1 \quad , \tag{3}$$

where R and a are, respectively, the major and minor plasma radii, m and n are the poloidal and toroidal wave numbers and $B_{0\theta}$ and B_{0_z} are the equilibrium magnetic field components in cylindrical coordinates (fig. 1). The mhd equilibrium is determined by the external uniform field B_{0_z} and the plasma current density

$$\vec{j} = j_0 \left[1 - \frac{r^2}{a^2}\right]^{\gamma} \hat{e}_z \quad , \tag{4}$$

where j_0 and γ are constants.

The field created by the currents I, flowing in opposite direction in the adjacent equally spaced helical windings, is conveniently described by the scalar potential ϕ expanded in harmonic series[13,14]; but for $r/R \ll 1$, as in the calculations here done, this field can be well approximated by a single harmonic in u:

$$\phi \simeq \frac{\mu_0\, I}{\pi} \left[\frac{r}{b}\right]^m \operatorname{sen} u \quad , \qquad \vec{B}_1 = \nabla \phi \tag{5}$$

where b is the tokamak vessel radius (fig. 1) and $u = m\theta - nz/R$.

The equations for the perturbed magnetic field lines are:

$$\frac{dr}{B_r} = \frac{r\,d\theta}{B_\theta} = \frac{dz}{B_z} \tag{6}$$

where the field components are known in terms of the coordinates r and u. The structure of the field line trajectories can be mapped on a z=const. plane and, as a consequence of this procedure, the Poincaré maps for these configurations are thus obtained.

In the limit $\epsilon \to 0$, the field $\vec{B}$ is integrable and there are magnetic surfaces described by a scalar function $\psi(r,u)$ constant along any field line, a property described by the differential equation:

$$\vec{B} \cdot \nabla \psi = 0 \quad . \tag{7}$$

The fig. 2a shows intersection of magnetic surfaces with a plane z=const. obtained for $\epsilon = 0$, $m = 3/n = 1$, $q(a) = 5$, $q(0) = 1$ and $I = 100$ A. In this case the perturbation $\vec{B}_1(r,3\theta-\phi)$ creates $m = 3$ magnetic islands around the resonant magnetic surface with $q = m/n = 3$.

When the correction of the magnetic field associated with the bending of the cylinder into a torus is introduced $(\epsilon \neq 0)$, eq. (7) is not valid anymore because the system's integrability is broken and magnetic surfaces are expected to be destroyed[12,14]. However, for a small helical perturbation, as considered in this paper, the major effect on a large aspect–ratio tokamak, due to the introduction of the mentioned toroidal correction, is the appearence of $m' = (m \pm i)$ $(i = 1, 2, ...)$ satellite magnetic islands within the rational magnetic surfaces with $q = (m \pm i)/n$. The overlapping of primary and secondary islands leads to the destruction of magnetic surfaces, and consequently to the appearence of chaotic regions in the plasma, as it can be seen in the example shown in fig. 2b. For $\epsilon = 0.27$, and considering the same equilibrium and helical perturbation of fig. 2a, this figure shows the presence of satellite islands – the $m' = 4$ and $m' = 2$ are the most noticeable ones – and chaotic regions between the islands.

To introduce toroidal correction in the field line equations (6), the external uniform component B_{0_z} (produced by a solenoid wound on a cylinder) is replaced by the field $B_{0_z}(1 + r/R \cos\theta)^{-1}$ produced by a solenoid wound on a toroidal camera with length $2\pi R$. If the new field line equations are expanded and the leading terms in ϵ are retained, the new terms, due to the toroidal corrections, are proportional to ϵ and I, which are therefore relevant control parameters in the present analysis. The dynamical

system described by these equations become symmetric, and therefore integrable, when the toroidal correction is neglible $(\epsilon \to 0)$ or the helical current vanish $(\phi \to 0)$. Thus, these differential equations characterize an almost integrable system[9], appropriate to be investigated by standard perturbation theories[8].

3. Destruction of Magnetic Surfaces

We integrated numerically the differential equations for different equilibria and several perturbation strenghts and outlined the Poincaré maps of the perturbed fields by plotting the successive intersections of several field line trajectories with a poloidal plane. Thus, these Poincaré maps consist of points (r_N, θ_N) such that

$$r_N = r_0 + \oint_0^{2\pi RN} \frac{dr}{dz}\, dz \tag{8}$$

$$\theta_N = \theta_0 + \oint_0^{2\pi N} \frac{d\theta}{dz}\, dz \quad . \tag{9}$$

These points correspond to the positions of a field line starting at (r_0, θ_0) after advancing by $2\pi\, R\, N$ $(N = 1, 2, 3, ...)$ along the z axis.

For a $q(0) = 1$ and $q(a) = 5$ mhd equilibrium and considering helical currents with helicity characterized by $m = 3/n = 1$, these maps show an expansion of the radial diffusion of any initial ensemble of points, taken in the region where $q \gtrsim 2$, for increasing perturbation strenghts.

In order to investigate the statistical properties of these maps, we analyse the evolution of the successive intersection coordinates (r_N, θ_N) of a given line with the plane

$z = 2\pi R N$ ($N = 1, 2, ...$) after N toroidal turns.

We followed the trajectories of a set of field lines choosing, on the map, starting points (r_0, θ_0) in the center of the area A determined by the circles with radii $r_{2/1}$ and $r_{3/1}$ (where $q(r_{m/n}) = m/n$). For all these lines, we collected the coordinates of their successive intersections (r_N, θ_N) and computed, for different values of S, the fraction $\alpha(S)$ of these intersections outside the area A (fig. 3). The diffusion of the intersections to regions outside this area become noticeable for $S > 0.7$ and increases with S until $S \simeq 1.1$, when the α values reach a saturated level and the intersections are scattered all over the chaotic area. To test the diffusion sensitivity to initial conditions, a typical characteristic of chaotic trajectories, the fluctuation levels σ_α in the computed α were also evaluated by changing slightly the original starting points (r_0, θ_0). The σ_α values become noticeable also for $S \tilde{>} 0.7$ and increase with S until $S \simeq 1.1$, the same behaviour observed for the α values. Thus, as it was observed for many others conservatives maps, the transition to chaos occurs in the interval $0.7 \tilde{<} S \leq 1.1$ [15,16].

Other algorithms were used to test the sensitive dependence on initial position, one of them, the Kolmogorov entropy k [8], computed as

$$k = \lim_{N \to \infty} \frac{1}{N} \sum_{i=1}^{N} \log \left| \frac{d(N)}{d(0)} \right| , \qquad (10)$$

is presented in the fig. 3c for two different line trajectories with two slightly different starting points separated by the distance $d(0)$ in the chaotic area. For the S values indicated in fig. 3, the m and $m' = m \pm 1$ islands are still present and, consequently, the decay of k with N present long tails and are not exponential, as it should be expected from investigations of long–time correlations of the chaotic regimes for two–dimensional periodic conservative maps[17,18].

To investigate the onset of chaotic field line trajectories we consider individual field line trajectories and analysed the sequence of their intersection coordinates (r_N, θ_N). As an example of our analysis, we consider in the following figures the line crossing the map on the starting point $(r_0 = 6.62$ cm, $\theta_0 = 0)$ for different helical current intensities I and $\epsilon = 0$ or $\epsilon = 0.27$.

Fig. 4a shows, in the large aspect–ratio limit $(\epsilon = 0)$, the sequence of r_N for $I = 10$ A; the periodic oscillation observed in this figure, and confirmed by the power spectrum in fig. 5b, is a consequence of the external periodic helical current. This periodicity determines also the regular projection of the four–dimension phase trajectory in the $r_N \times v_N$ plane (fig. 5a), where v_N is defined as

$$v_N = \frac{dr}{dz}(r_N, \theta_N) . \qquad (12)$$

Figs. 5c and 5d show, for the same value of I, as in the previous case, but considering the mentioned toroidal correction $(\epsilon = 0.27)$, the onset of a second period due to the $\cos\theta$ dependence on the equilibrium $\vec{B}_0$ field. The phase trajectory projection shown in fig. 5c is comparable to projections obtained in the chaos onset analysis of other dynamical systems with non–linear coupling[19]. For this case, using I values ranging from very low helical current intensities to $I \tilde{<} 20$ A, the projections were found to be very similar for different perturbations intensities and their lengths scales with I. However, for higher values of I, the projection deformations increase with I, although the trajectories still preserve global resemblance with those obtained at low current intensities, as it can be seen in figs. 6a and 6b for $I = 80$ A. Above 100 A $(S > 1)$, the analysed projections and their power spectra are both typical of chaotic trajectories[19]. In this case, currents with approximatly same intensities lead not to similar projections (figs. 6c and 6d), as noted for lower strenght helical perturbations, showing sensibility to small changes on this control parameter I.

The comparison of several power spectra, like those here presented, strongly suggested the coupling between the $m = 1$ toroidal correction and the $m = 3/n = 1$ helical perturbation as the responsible for the onset of chaotic trajectories with their broadband spectra. Other starting points (r_0 , θ_0) lead to resembling evolutions with I, but with other patterns in the plane $r_N \times v_N$ (see the fig. 7a and 7b).

Finally, we present an example of the r_N evolution for starting points inside the primary magnetic islands (localized around the unperturbed surface with $q = 3$) neglecting and taking into account the toroidal correction (fig. 8). In these cases, the generated intersections remain all inside the three primary islands and, for $\epsilon = 0.27$, we notice a smaller r_N oscillation amplitude a consequence of islands destruction caused by their superposition[8].

4. Conclusions

The ontset of chaotic magnetic field line trajectories was numerically investigated, for tokamak mhd equilibria perturbed by resonant helical windings, considering the external helical current as a relevant control parameter in the experience considered in this article. To analyse this transition, the perturbed differential equation was integrated to obtain field lines Poincaré maps and phase space line trajectories. Qualitative changes in these maps and trajectories show, as observed for other conservative maps, chaos transitions in the interval $0.7 \tilde{<} S \tilde{<} 1.1$. In this interval, comparisons of quasi–periodic and irregular field lines revealed the enhancement of the coupling between the $m = 1$ toroidal correction and the m/n helical perturbation, as the helical current increased and the stochasticity parameter approuched the value $S \tilde{=} 1$.

Acknowledgments

The authors would like to thank discussions with Dr. Marco Brusati (JET) and Dr. Álvaro Vannucci (IFUSP).

Refenrences

1. H. Grad; *Int. J. Fusion Energy* **3**, 33 (1985).
2. M.Y. Kucinski, I.L. Caldas, L.H.A. Monteiro and V. Okano; *J. Plasma Phys.* 44, 303 (1990).
3. D.C. Robinson; *Nucl. Fus.* 25, 1101 (1985).
4. F. Karger and O. Kluber; *Nucl. Fus.* 25, 1059 (1985).
5. S.C. McCool et al.; *Nucl. Fus.* 29, 547 (1989).
6. M.N. Rosenbluth, R.Z. Sagdeev, J.B. Taylor, G.M. Zaslavski; *Nucl. Fus.* **6**, 297 (1966).
7. J.M. Finn; *Comments Plasma Phys. Contr. Fus.* **14**, 149 (1991).
8. A.I. Lichtenberg and M.A. Lieberman; "Regular and Stochastic Motion", Springer Verlag, New York (1983).
9. M.V.A.P. Heller, I.L. Caldas and M.C.R. Andrade; "Almost Integrable Magnetic Field in Tokamaks, in Nonlinear Phenomena in Fluids, Solids and Other Complex Systems", P. Cordero and B. Nachtergaele (editors), Elsevier Science Publishers B.V., 83, Amsterdam (1991).
10. A. Vannucci, O.W. Bender, I.L. Caldas, I.H. Tan, I.C. Nascimento and E.K. Sanada; *Nuovo Cimento* **10D**, 1193 (1988).
11. A. Vannucci, I.C. Nascimento and I.L. Caldas; *Plasma Phys. and Contr. Fus.* **31**, 147 (1989).
12. J.M. Finn; *Nucl. Fus.* **15**, 845 (1975).
13. A.I. Morozov and S.L. Solov'ev; *Reviews of Plasma Phys.* (edited by M.A. Leontovich), Vol. 2, 1, Consultants Bureau, New York (1966).
14. A.S. Fernandes, M.V.A.P. Heller and I.L. Caldas; *Plasma Phys. Contr. Fus.* **30**, 1203 (1988).
15. I.C. Percival; *Proc. of the Royal Society of London* **413**, 131 (1987).

16. P.H. Rebut, M. Brusati, M. Hugon, P.P. Lallia; "Proc. 11th Int. Conf. Plasma Phys. Thermonuclear Fus." (Kyoto, 1986) **II**, 187, IAEA, Viena (1987).
17. J.D. Meiss, J.R. Cary, C. Grebogi, J.D. Crawford, A.N. Kaufman and H.D.I. Abarbanel; *Physica* **6D**, 375 (1983).
18. C.F.F. Karney; *Physica* **8D**, 360 (1983).
19. R.S. Mackay and J.D. Meiss; "Hamiltonian Dynamical Systems", Adam Hilger, Bristol (1987).

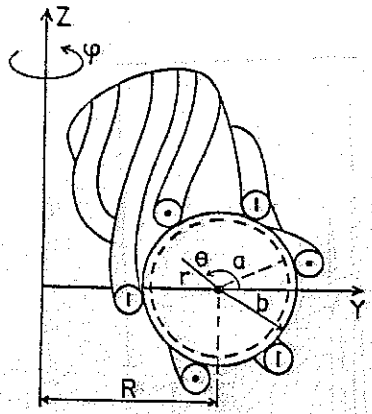

Fig.1 - Coordinate system (r,θ,φ) and outline of the helical windings on the toroidal camera.

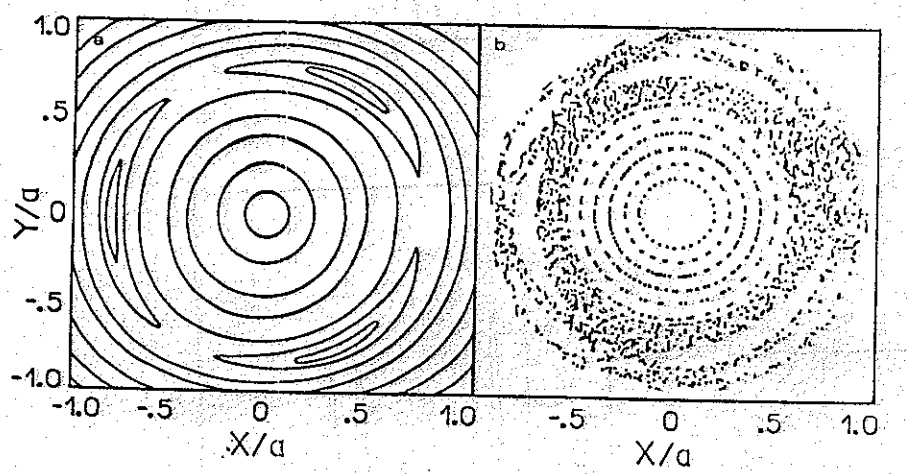

Fig.2 - Perturbed Poincaré map on the poloidal plane $z = 2\pi R(N = 0,1,2,\ldots)$ for an integrable field, $\epsilon = 0$, (2a); I = 100 A, q(0) = 1 and q(a) = 5. The same, taking into account the toroidal correction, $\epsilon = 0{,}27$ (2b).

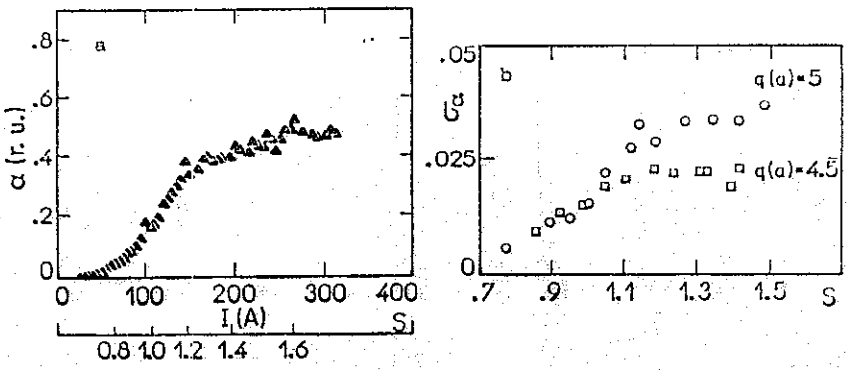

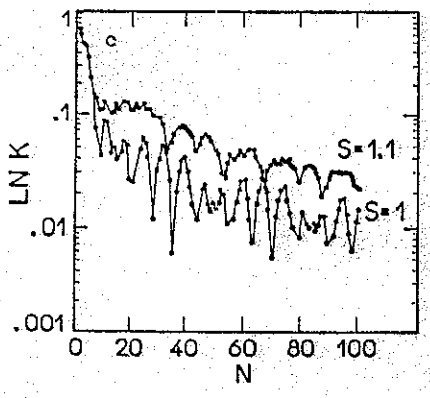

Fig.3 - Variation of the fraction α as a function of the helical current I and S (for q(0) = 1 and q(a) = 5) for $\epsilon = 0{,}27$ (a). Standard deviation of the α computed values distribution as a function of S for two different values of q(a) (b). Kolmogorov entropy computed for initial coordinates in the chaotic area of the map shown in the fig.2b, I = 100 A (S = 1), and for the map obtained for I = 110 A (S = 1.1)(c).

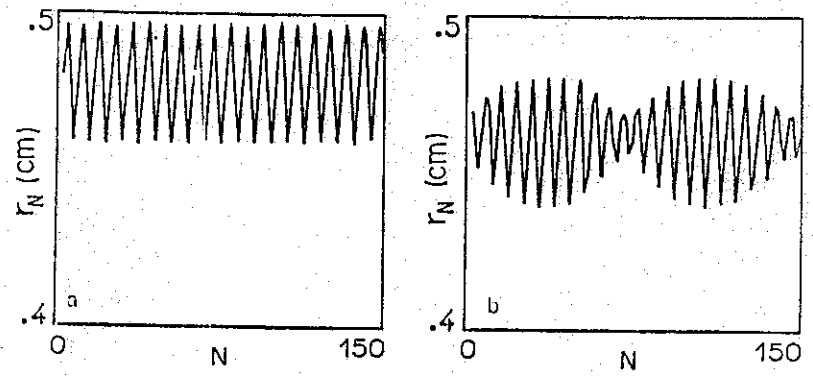

Fig.4 - Radial coordinates of N sucessive interactions on the Poincaré map for a given field line trajectory (r_o=6.62 cm, θ_o= 0), I = 10 A and $\epsilon = 0$ (a) and $\epsilon = 0.27$ (b).

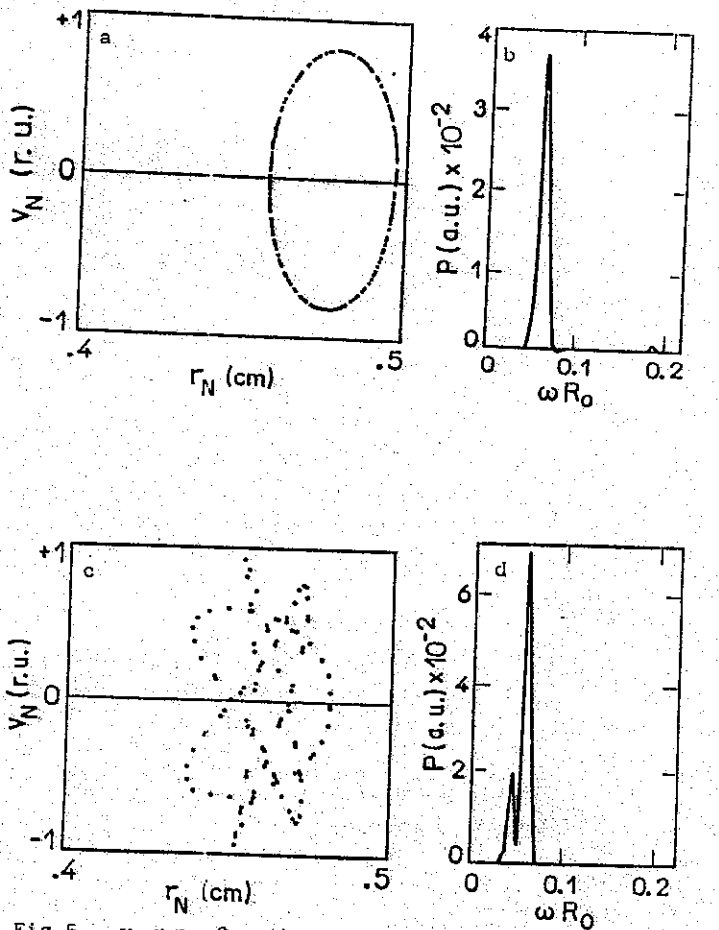

Fig.5 - $v_N \times r_N$ for the same conditions of the fig.4a, $\varepsilon = 0$ (a) and the corresponding power spectrum of $v_N \times N$ (b). The same for $\varepsilon = 0.27$ (c,d).

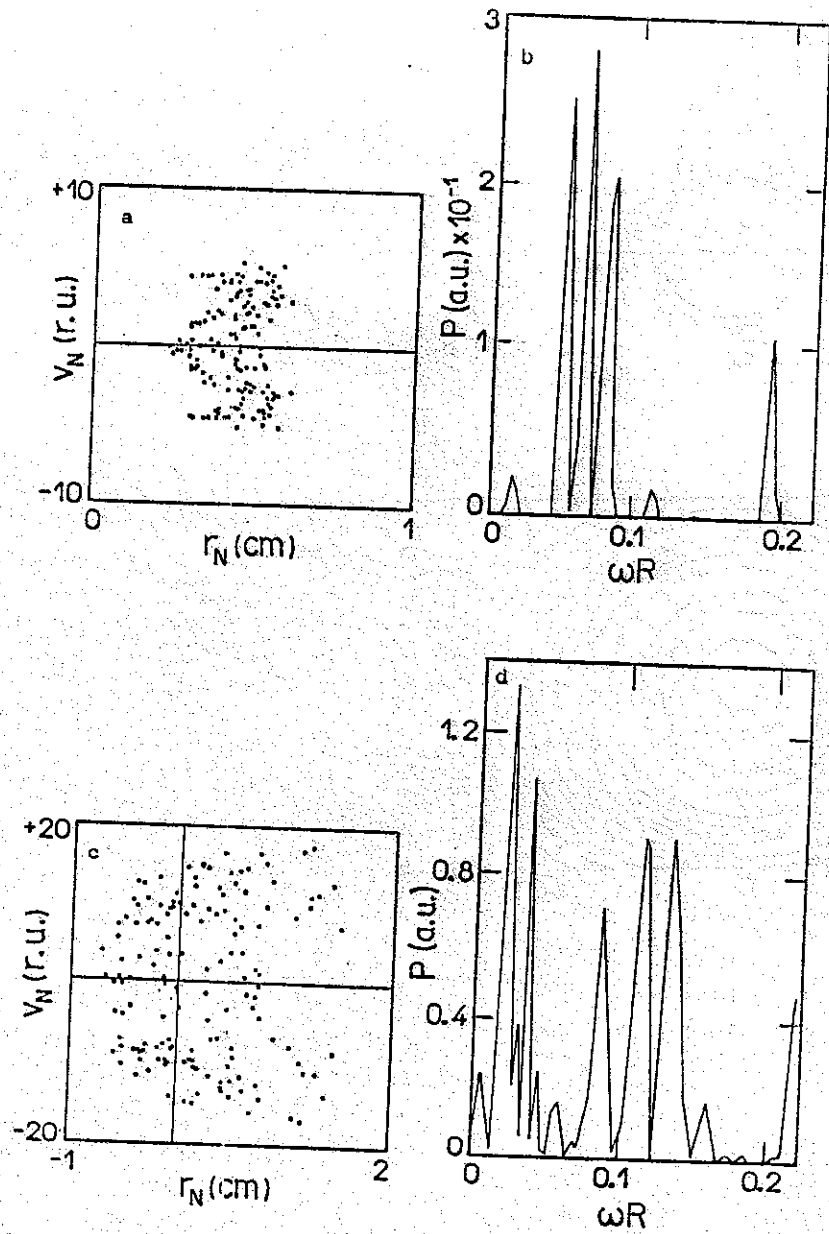

Fig.6 - $v_N \times r_N$ for the same conditions of the fig.5a, $\varepsilon = 0.27$, and their $v_N \times N$ power spectra for I = 80 A (a,b) and I = 200 A (c,d).

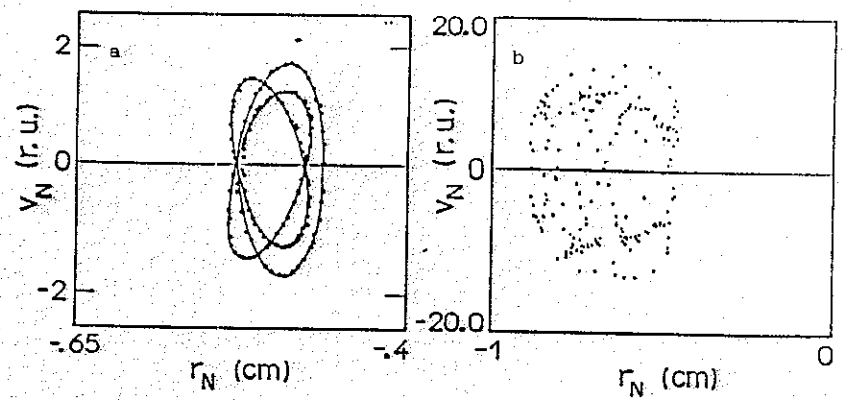

Fig.7 - $v_N \times r_N$ for a field line with $r_o = 5.7$ cm and $\theta_o = 0$, $\epsilon = 0{,}27$, I = 10 A (a) and I = 200 A (b).

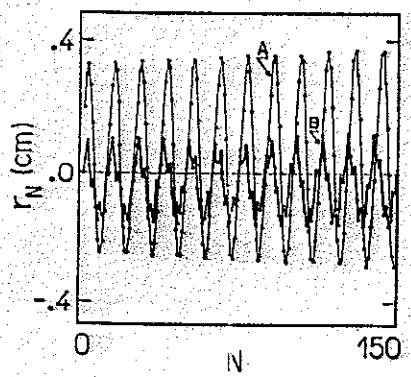

Fig.8 - Radial coordinates of N sucessive interactions on the Poincaré map for a field line trajectory ($r_o = 6{,}62$ cm, $\theta_o = 80^o$), inside a magnetic island, for $\epsilon = 0$ and (curve A) $\epsilon = 0.27$ (curve B).